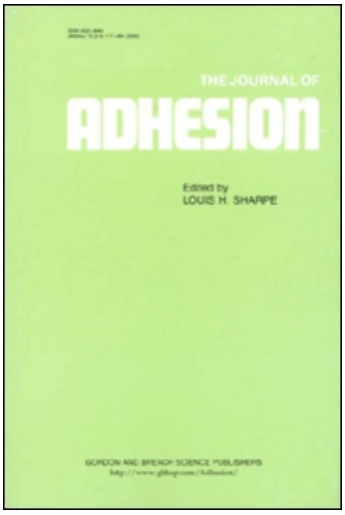

The Journal of Adhesion

Publication details, including instructions for authors and subscription information:
http://www.informaworld.com/smpp/title~content=t713453635

A Stress Singularity Approach for the Prediction of Fatigue Crack Initiation in Adhesive Bonds. Part 2: Experimental

D. R. Lefebvre[a]; D. A. Dillard[a]; J. G. Dillard[b]
[a] Engineering Science and Mechanics Department, Virginia Polytechnic Institute and State University, Blacksburg, USA [b] Chemistry Department, Virginia Polytechnic Institute and State University, Blacksburg, USA

To cite this Article Lefebvre, D. R. , Dillard, D. A. and Dillard, J. G.(1999) 'A Stress Singularity Approach for the Prediction of Fatigue Crack Initiation in Adhesive Bonds. Part 2: Experimental', The Journal of Adhesion, 70: 1, 139 — 154
To link to this Article: DOI: 10.1080/00218469908010491
URL: http://dx.doi.org/10.1080/00218469908010491

J. Adhesion, 1999, Vol. 70, pp. 139–154
Reprints available directly from the publisher
Photocopying permitted by license only

A Stress Singularity Approach for the Prediction of Fatigue Crack Initiation in Adhesive Bonds. Part 2: Experimental*

D. R. LEFEBVRE[a,†], D. A. DILLARD[a] and J. G. DILLARD[b]

[a]*Engineering Science and Mechanics Department, Virginia Polytechnic Institute and State University, Blacksburg, VA 24061, USA;*
[b]*Chemistry Department, Virginia Polytechnic Institute and State University, Blacksburg, VA 24061, USA*

(Received 30 May 1998; In final form 17 December 1998)

Using the epoxy-aluminum wedge specimens defined and analyzed in Part 1, we measure the number of cycles required to initiate an interfacial fatigue crack near the apex, where the stress field is predicted to be singular. The eigenvalue, λ, and the generalized stress intensity factor, Q, are varied *via* the wedge angle, and *via* the beam deflection, respectively. Crack initiation is detected using a strain gage bonded near the tip of the wedge.

Following the methodology developed in Part 1, the fatigue data are then used to construct a fatigue initiation criterion characteristic of the bimaterial interface. This criterion is a 3-D surface, with the ordinate representing the generalized stress intensity factor and the two horizontal axes representing the number of cycles to initiation and the eigenvalue, respectively. Three key assumptions of the model are found to be satisfied in the specimens tested herein: (1) geometric imperfections at the apex are smaller than the singular region, (2) the plastic zones near the apex are also smaller than the singular region, and (3) the locus of initiation is near interfacial.

Finally, a thermomechanical analysis indicates that the residual thermal stresses generated during the fabrication process make a significant contribution to the critical stress intensity factor. With high T_g adhesives and under unfavorable conditions (high modulus, high CTE, poor adhesion), we predict that the residual stresses alone could be sufficient to cause debond initiation.

---

* Presented at the 21st Annual Meeting of The Adhesion Society, Inc., Savannah, GA, USA, February 22–25, 1998.

†Address for correspondence: Motorola/AIEG, 4000 Commercial Avenue, Northbrook, IL 60062-1840, USA. Tel.: 847-480-8044, Fax: 847-205-3804, e-mail: G15010@email.mot.com

Keywords: Adhesive bond; fatigue; durability; debond initiation; bimaterial wedge; bimaterial interface; singular stress field; generalized stress intensity factor; thermal residual stresses; plastic zone

INTRODUCTION

In Part 1 of this study [1] we discussed how fatigue cracks in adhesive joints tend to initiate near interface corners where the stress field is predicted to be singular, and we defined a 3-D fatigue initiation surface using a *single* generalized stress intensity factor, Q, and a single singular eigenvalue, λ. The validity domain of the criterion was defined as follows: a modulus ratio (adhesive-to-adherend) smaller than 0.1 and interface apex angles smaller that 90°; all of which were satisfied in the case of the epoxy-aluminum wedge specimens designed for our experimental study.

In Part 2, we describe the fabrication and fatigue testing of the aluminum-epoxy wedge specimens described in Part 1. Individual Q *vs.* (number of cycles to debond initiation) curves corresponding to discrete values of λ are presented, which we then use to construct the delamination surface conjectured in Part 1. Thermal residual stresses are taken into account in the computation of Q and their potential role in pre-cracking is discussed. In addition, to ensure that the key assumptions of the criterion are satisfied, we investigate the sharpness of the epoxy wedges, the scale of the plastic zone, and the locus of crack initiation.

SPECIMEN GEOMETRY

The specimens consisted of 60 mm long epoxy wedges cast onto flat aluminum beams ($220 \times 15 \times 3.175$ mm). Three wedge angles were used: 55°, 70° and 90°, yielding single eigenvalues of 0.09, 0.19 and 0.30, respectively [1]. The specimen dimensions and wedge angles are shown in Figure 1.

MATERIALS AND SURFACE TREATMENT

The wedges were made of diglycidyl ether of bisphenol-F (DGEBF) Epon 862™ cured with 14.2 phr triethelenetetramine (TETA), both

supplied by Shell Chemical Company. The cure cycles was 5 days at room temperature, followed by a post-cure at 125°C for 1 hour. The beams were made of 6061 T6 aluminum cleaned with an acid-base treatment, followed by a P2 etch [2] (aqueous solution of ferric sulfate and sulfuric acid). The material properties are listed in Table I.

SPECIMEN FABRICATION

The epoxy wedges were cast onto the aluminum beams, using silicone rubber molds (General Electric's RTV 664) featuring the negatives of the three different specimen geometries. The rubber molds were made from a primary mold holding precision-machined steel templates of the three different wedge geometries. This technique allowed us to fabricate inexpensively enough rubber molds to make all of the 90 specimens needed for a complete fatigue study from a single batch of surface

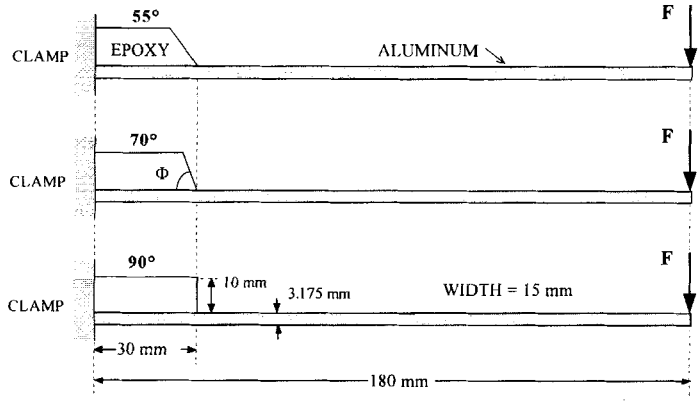

FIGURE 1 Specimen geometry and actual dimensions.

TABLE I Materials properties: modulus, Poisson's ratio and coefficient of thermal expansion

	Young's Modulus (GPa)	*Poisson's ratio*	*CTE (ppm/°C)*
Aluminum 6061 T6	69	0.30	25
Epon 862 – TETA	3.2	0.35	61

treatment solutions, thus eliminating a source of scatter and reducing fabrication time.

After mixing with the curing agent and degassing in a vacuum chamber, the epoxy was cured as described previously. Clear, bubble-free wedges with sharp angles were obtained. The sharpness of the wedge tip was measured using polished SEM sections. A magnified view of the interface corner of a debonded 70° specimen is shown in Figure 2. Note that the geometry of the tip deviates from a perfect right angle by only about 20 μm. The geometrical defect is thus 4 times smaller than the calculated size of the singular zone, meeting a key requirement of the stress singularity approach [1]. With a few exceptions, the same sharpness scale was found in the 55° and 70° specimens.

Using an MTS servohydraulic machine driven in *displacement* control, the wedge specimens were loaded in bending. Because of the large number of data points required to generate a given failure envelope, it was highly desirable to have a fixture capable of testing several specimen at the same time. Simultaneous testing of 8 specimens was

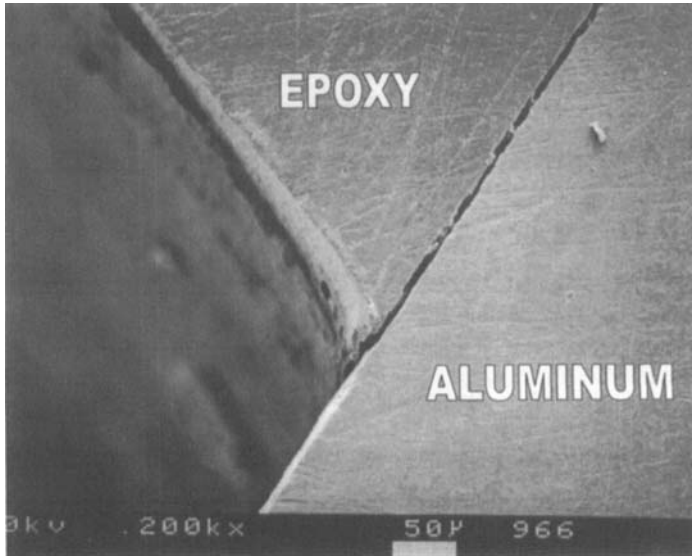

FIGURE 2 SEM micrograph of the interface corner of a debonded 70° wedge specimen. Magnification: 200X.

achieved using a fixture consisting of two major components: (1) a circular hub capable of clamping 8 specimens (oriented as the spokes of a wheel) and (2) a second hub holding 8 rigid beams oriented parallel to the specimens. Bolted to the extremities of the rigid beams were tups whose vertical positions could be independently adjusted. The hub holding the rigid beams was bolted to the fixed crosshead of the MTS frame, while the hub holding the specimens was bolted to the MTS actuator. This design is illustrated in Figure 3, showing only 1/8th of the "octopus" shaped fixture and in Figure 4 showing the entire fixture.

The fatigue loading was a sinusoidal waveform with a frequency of 5 Hz. The maximum and minimum deflections were always downward, ensuring continuous contact between the tups and the aluminum substrates. The load-ratio (min/max) was 0.2. The environment was room temperature air. The deflection of the beam was kept within the elastic range of the aluminum.

CRACK INITIATION DETECTION

Crack initiation detection was achieved using a strain gage bonded near the apex of the epoxy wedge (see Fig. 3). The strain gage was connected to full Wheatstone bridge circuits. After amplification and

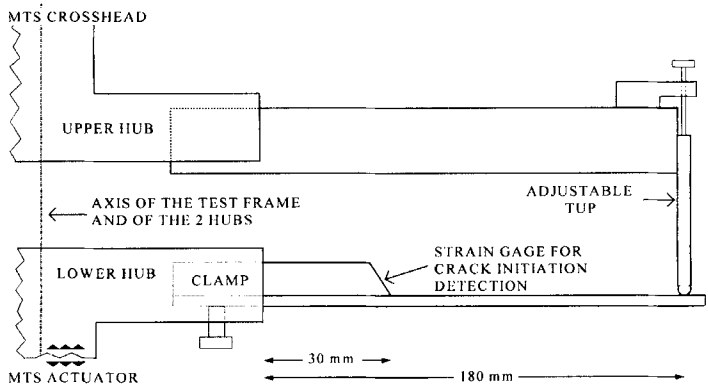

FIGURE 3 Experimental fixture. The schematic shows 1 of 8 specimens that can be mounted around the hubs.

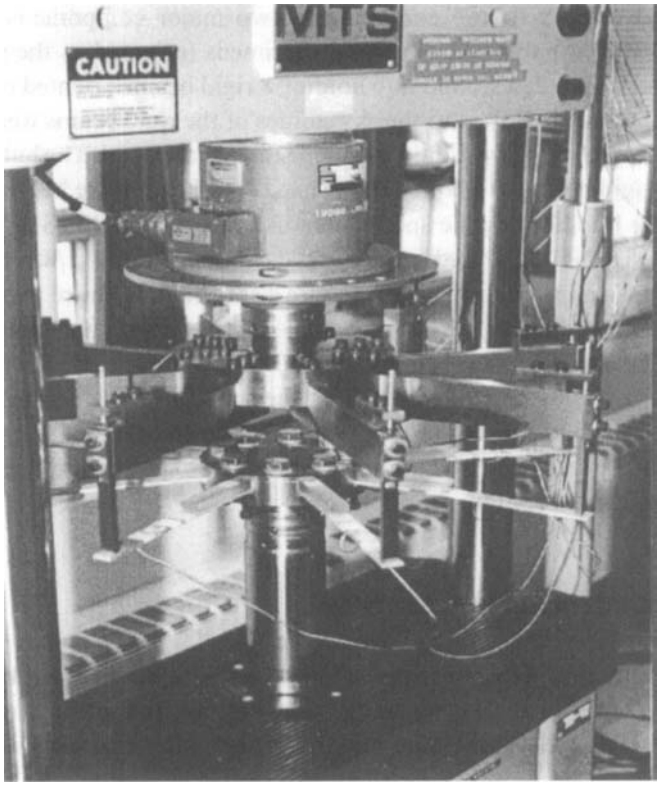

FIGURE 4 8 Specimens mounted on the "Octopus"-shaped fixture.

digital conversion, the signals from the strain gages were recorded by a LABVIEW™ program running on a desktop computer. At specified time intervals, the program would acquire two periods of the sinusoidal signal, determine its extrema, and plot its range as a function of the number of elapsed cycles. Whenever a crack would initiate, the surface strains near the apex of the wedge would drop, causing a decrease in the range of the sinusoidal signal from the strain gage. A similar technique has been used to detect crack initiation near weld toes [3] and in single-lap joints [4].

An example of data acquisition and analysis is given in Figure 5. The ordinate represents the range of the sinusoidal waveform measured with the strain gage. The abscissa represents the number of elapsed cycles. The number of cycles to initiation was obtained graphically

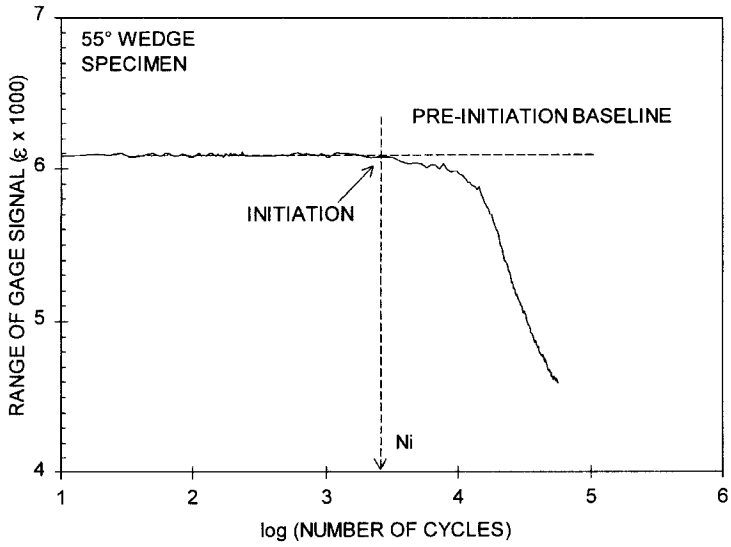

FIGURE 5 Example of data acquisition from the strain gage. N_i = number of cycles to initiation.

as shown in Figure 5. Because the error associated with the graphical method was small compared with the scatter originating from fatigue strength variations, a more elaborate technique was deemed unnecessary.

SPECIMEN CALIBRATION

Using the plane stress linear elastic finite element analysis (ABAQUS™) described in Part 1 [1], we calculated Q_{yy} *vs.* beam deflection for the 3 selected wedge specimen geometries (55°, 70° and 90°). This relationship was used to calibrate our fatigue tests to be carried out in *displacement* control. Q_{yy} was calculated from the peel stress distribution along the *interface*. Q_{VM} (Q from the Von Mises stress distribution) as a function of deflection was also determined to help estimate the size of the plastic zone as discussed in Part 1. Q_{VM} was calculated using the Von Mises stress distribution along several rays crossing the epoxy corner and was found to be virtually independent of ray angle.

The thermal residual stresses generated during specimen fabrication were taken into account in the calibration. Their contribution to the generalized stress intensity factor was evaluated using a thermomechanical analysis in ABAQUS™. The coefficients of thermal expansion of the two materials are listed in Table I. Assuming that the anchoring temperature of the epoxy was equal to its glass transition temperature (105°C [5]), we found that the residual stresses built up over a temperature drop (ΔT) of about 80°C. We obtained the same value of ΔT independently from beam curvature measurements performed at room temperature on freshly-made specimens. With this alternate method, ΔT was obtained by using the classical thermostat solution derived by Timoshenko [6].

As discussed in Part 1 [1], Q from a thermomechanical loading can be expressed as the sum of a purely thermal component and of a remote mechanical deflection component, leading to the following calibration relationship:

$$Q = Q_{kl}^{th} + b\delta \tag{1}$$

where:

Q_{kl}^{th} = Thermally-induced Q
b = Constant (linear analysis only)
δ = Beam deflection

The calibration constants obtained numerically are listed in Tables II and III.

EXPERIMENTAL RESULTS

The Q *vs.* N_i curves for each of the 3 selected values of λ are presented in Figures 6 to 8 on semi-log plots. The thermal stress correction was included in the computation of Q. Note that two different scales are shown on the ordinate: one for ΔQ, and one for Q_{max}, where:

Q_{min} = Minimum Q_{yy}
Q_{max} = Maximum Q_{yy}
$\Delta Q = Q_{max} - Q_{min}$ (range)

TABLE II Q_{yy} Calibration. σ_{yy} was calculated along the interface

Wedge Angle	55°	70°	90°
Thermally induced Q_{yy} (MPa mm$^{\lambda}$)	9.9	11.0	9.3
b (MPa mm$^{\lambda-1}$)	1.3	1.9	2.0

TABLE III Q_{VM} Calibration. Q_{VM} was calculated from the Von Mises stress distributions along various rays within the epoxy block

Wedge Angle	55°	70°	90°
Thermally induced Q_{VM} (MPa mm$^{\lambda}$)	15.8	14.3	10.4
b (MPa mm$^{\lambda-1}$)	2.2	2.5	2.4

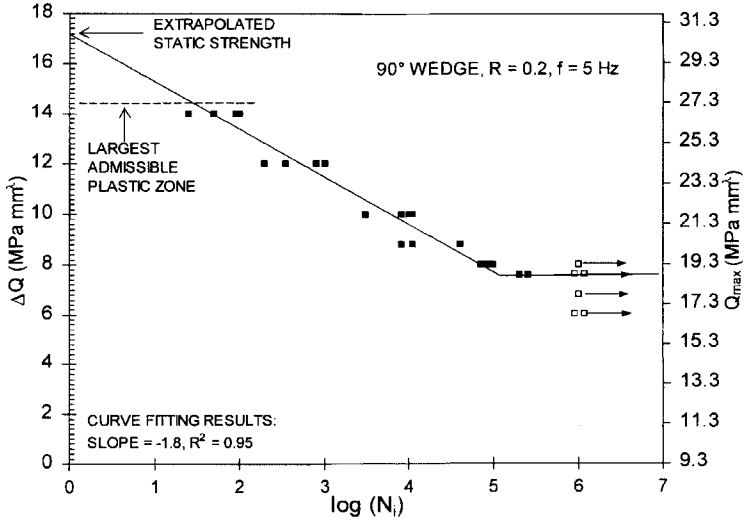

FIGURE 6 $Q-N_i$ curve for a 90° wedge specimen. $\lambda = 0.30$, $R = 0.2, f = 5$ Hz. Q was calculated from σ_{yy}.

Whenever initiation had not occurred at 10^6 cycles, testing was interrupted and the data points were represented as open squares with arrows pointing to the right. For all three values of λ, the $Q-N_i$ curves seemed to reach an asymptote before 10^6 cycles, suggesting the existence of an endurance limit. To facilitate future statistical treatment, several points were collected for each ΔQ level. Data points with a N_i smaller than 10 (2 seconds of testing at 5 Hz) could not be

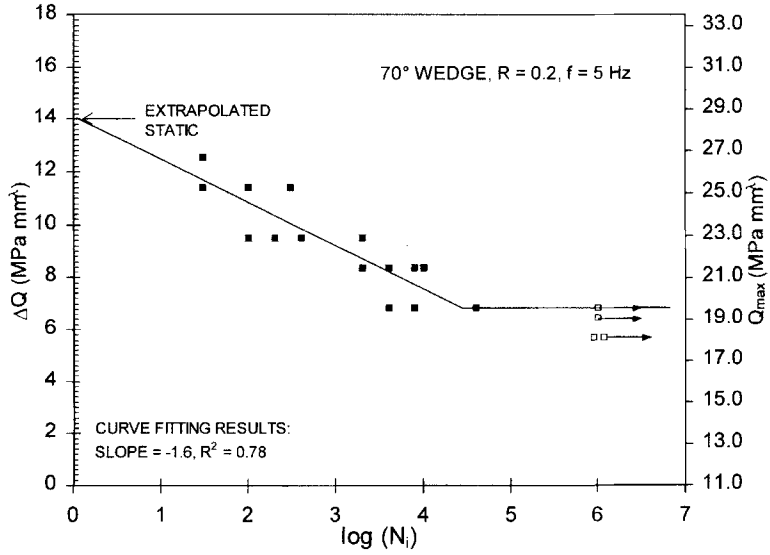

FIGURE 7 $Q-N_i$ curve for a 70° wedge specimen. $\lambda = 0.19$, $R = 0.2$, $f = 5$ Hz. Q was calculated from σ_{yy}.

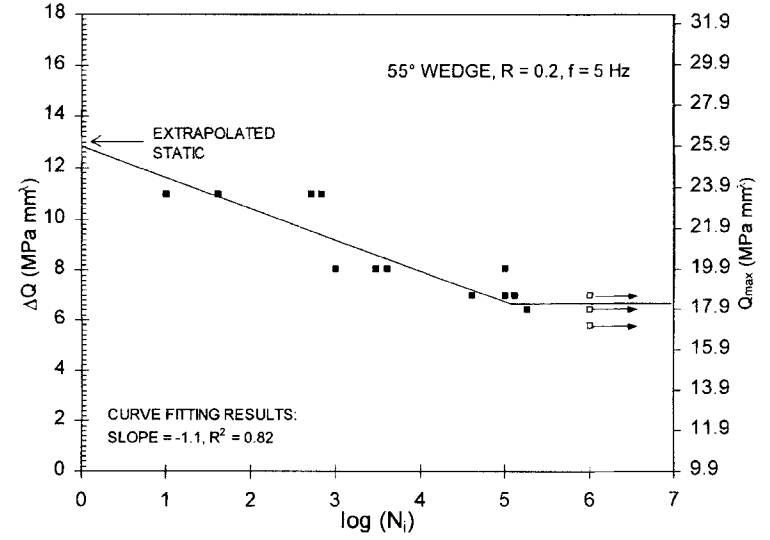

FIGURE 8 $Q-N_i$ curve for a 55° wedge specimen. $\lambda = 0.09$, $R = 0.2$, $f = 5$ Hz. Q was calculated from σ_{yy}.

collected, because it was not possible to define a clear pre-initiation baseline (see Fig. 5) with so few data points. For this reason, the low cycle fatigue portions of the curves were only extrapolations.

The data points situated *above* the fatigue limit were curve-fitted to a relation of the type: $\Delta Q = \Delta Q_0 - \alpha \log(N_i)$ by linear regression. In view of the scatter, the slopes can be considered to be virtually identical. The fatigue limit at 10^6 cycles is also quasi-independent of λ. The scatter along the N_i axis increased markedly as λ decreased.

Role of Thermal Stresses

Beam curvature did not decrease with time, indicating that *far field* residual thermal stresses did not relax over time. However, uncertainty does remain about what really happens near the singular point where stresses are extremely high. A paper by Reedy *et al.*, clearly suggests this possibility [7]. Thus, future research may reveal that the thermal correction proposed in this paper is too simplistic. Nevertheless, in the absence of a definite answer, and for the sake of simplicity, we will assume for now that near field stresses did not relax.

Since, for $\Delta Q = 0$, $Q_{\max}$ is entirely due to residual stresses, the comparison of the 2 vertical axes on the various $Q - N_i$ curves provides valuable insight on the role of thermal stresses. From Table IV, we see that thermal stresses accounted for as much as 55% of Q_{yy} at the fatigue limit, and as much as 38% of Q_{yy} at static strength (extrapolated).

The significant contribution of residual thermal stresses to the generalized intensity factor raises the possibility that, with high T_g adhesives, crack initiation could occur during the fabrication process. Assuming that both the adhesive modulus and adhesion remained

TABLE IV Contribution of thermal residual stresses to Q_{yy} (from FEA). The corresponding maximum beam deflection is listed in parenthesis

	Contribution of Thermal Stresses to Q_{yy} at Static Strength (Extrapolated)	*Contribution of Thermal Stresses to Q_{yy} at the Fatigue Limit*
90° Wedge	30% (δ = 11.25 mm)	48% (δ = 4.75 mm)
70° Wedge	37% (δ = 10.50 mm)	55% (δ = 4.50 mm)
55° Wedge	38% (δ = 12.1 mm)	53% (δ = 6.13 mm)

constant, our numerical simulations indicated that ΔT would have had to be of the order of 200°C to trigger spontaneous delamination at room temperature. This places the T_g of such an adhesive in the 200–220°C range. With such a high T_g adhesive system, it would seem advantageous to reduce the CTE through compounding.

Another effect of the thermal stresses was to render the *actual* R ratio ($R = Q_{\min}/Q_{\max}$) load dependent. Although far from ideal, this situation is not unusual in weld fatigue testing, where the nominal stress plotted on the $S-N$ curve does not take into account residual stresses within the thermally affected zone.

3-D Initiation Envelope

The linear regressions obtained from the three preceding $Q-N_i$, plots were collected to construct a portion of the 3-D initiation envelope conjectured in Part 1 [1]. The resulting failure surface is shown in Figure 9. The ordinate represents ΔQ_{yy} and the two horizontal axes represent $\log(N_i)$ and λ, respectively. This initiation criterion is characteristic of the aluminum-epoxy bimaterial interface, including

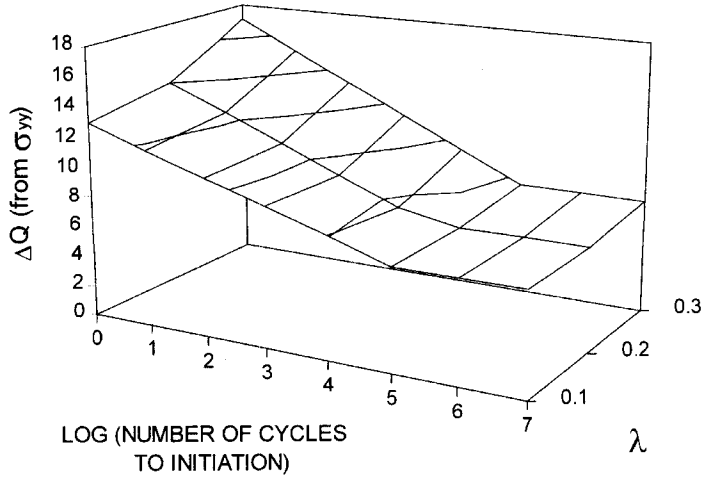

FIGURE 9 Delamination envelope characteristic of the P2-Etched Al 6061-T6/DGEBF-TETA bimaterial interface. $R = 0.2, f = 5$ Hz, room air.

the surface treatment. It is also dependent on the R ratio, on the test environment, and on frequency (weakly so with glassy polymers, as long as heat build-up is negligible). The main potential advantage of this criterion lies in the fact that it is theoretically independent of geometry and loading conditions [1].

Figure 9 shows that, within the range of eigenvalues investigated, the $Q-N_i$ curves and the fatigue limits did not vary considerably. It is also noteworthy that for $N_i = 1/4$ (static failure), the extrapolated critical Q *decreased* with λ, following the opposite trend to that observed by Hattori [8] for a filled epoxy bonded to an Fe–Ni substrate.

Locus of Initiation

In the vast majority of cases, delamination did not initiate near the edges of the beam. Rather, it initiated away from the beam edges, where the anticlastic effect generates higher peel stresses [9]. Since Our 2-D analysis could not take into account edge effects, this situation was rather fortunate. Paradoxically, the 2-D plane stress analysis could not model the anticlastic effect either. In spite of this limitation, the plane stress approximation is believed to be reasonable.

XPS analysis of the failure surface in the initiation area showed strong elemental peaks from both the aluminum and the epoxy, indicating that initiation was "mixed mode", right at the aluminum-epoxy interface. Thus, the requirement of the stress singularity approach, that initiation be interfacial, was fulfilled.

With wedges made of a room temperature adhesive formulation[1] (*i.e.*, no residual thermal stresses), we observed that cracks could sometimes initiate *cohesively* near the apex of the wedge, in a direction perpendicular to the maximum principal stress. We speculate that this phenomenon at initiation is analogous to the crack path selection mechanism described in the propagation phase [10], namely that the tensile thermal residual stresses in the epoxy may have steered the crack in the direction of the interface.

[1]Epon 828, Jeffamine D-230 (32 phr), Huntsman Accelerator 399 (2 phr).

ESTIMATION OF THE SIZE OF THE PLASTIC ZONE

Using the calibration data, we estimated that in the case of the 90° wedge specimen, the maximum Q_{VM} attained during testing was 30 MPa. With an epoxy yield strength of 83 MPa [5], this stress level generated a plastic zone size of 80 μm, *i.e.*, barely under the 100 μm size of the singular zone. Around the fatigue limit of the 90° wedge specimen, the same procedure gave a plastic zone size of 30 μm. Similar estimates for wedge angles of 70° and 55° gave much smaller plastic zones. A summary of all these results is given in Table V.

Since the plastic zone size approximations were conservative (see Part 1), the results listed in Table V allowed us to conclude with a fair level of confidence that the plasticity requirement of the singular approach was satisfied for most, if not all, fatigue data points collected in this study.

In the case of the 90° wedge, the size of the plastic zone associated with the extrapolated static strength exceeded that of the singular zone (see the horizontal dashed line in Fig. 6). By contrast, no oversize plastic-zone was predicted for the 70° and 55° wedges, even at the extrapolated static strength levels.

The fatigue behavior of the 90° wedge specimen is also very interesting, in that it illustrates that the stress singularity approach can be applicable at loads close to the fatigue limit, even when the plastic zone exceeds the size of the singular region at static failure loads. Remarkably, because of the very steep power law governing the size of the plastic zone [1], the difference in stress level between the static

TABLE V Conservative estimate of the size of the plastic zones, from Eq. (7) in Part 1 ($\gamma = 2$, $\sigma_{yd} = 83$ MPa). The size of the plastic zone should be compared with that of the singular region (100 μm)

	Maximum Load Reached During Fatigue Testing		*Load Corresponding to the Fatigue Limit*	
Wedge Angle ↓	*Maximum* Q_{VM}	*Estimated Size of the Plastic Zone*	*Maximum* Q_{VM}	*Estimated Size of the Plastic Zone*
90°	31 MPa	80 μm	22 MPa	30 μm
70°	35 MPa	20 μm	26 MPa	5 μm
55°	42 MPa	1 μm	30 MPa	0.02 μm

strength and the fatigue strength does not need to be very large for this kind of dual situation to exist.

CONCLUSIONS

A fatigue initiation criterion based on the use of a single generalized stress intensity factor seems achievable, provided the following requirements are met:

- Adhesive-adherend corner angles no larger than 90°.
- A modulus ratio (adhesive-to-adherend) smaller that 0.1.
- An interfacial locus of initiation.
- A singular zone significantly larger than the plastic yield zone, intrinsic flaw size and geometric imperfections at the apex.

The obtained delamination envelope is a 3-D generalization of Hattori's 2-D static criterion. It is characteristic of a given bimaterial interface, including the surface treatment. From theory, this envelope is predicted to be independent of loading and geometry. In the case of the epoxy-aluminium bond investigated in this study, a fatigue limit at 10^6 cycles could be defined. When expressed in terms of ΔQ, this fatigue limit was virtually independent of the order of the singularity.

It is not completely clear at this point whether residual stresses near the singular point undergo relaxation (far-field thermal stresses did not). Even if they did relax, they would still play a major role in the initiation process in the case of freshly fabricated adhesive bonds.

The formation of a plastically-yielded zone near the apex of the adhesive-adherend corners can limit the applicability of the stress singularity approach, especially at the higher loads associated with static failure. Fortunately, because the power law governing the size of the plastic zone tends to have large exponents, the stress singularity approach is likely to be applicable at loads corresponding to the fatigue limit, even if that is not the case at loads associated with the static strength. In addition, the estimated size of the plastic zone decreases sharply as the adhesive contact angle decreases. If confirmed, this result would mean that the blunting of crack initiation by the formation of a plastic zone larger than the singular region is less likely as the adhesive contact angle decreases.

Our $Q - N_i$ curves indicate that Q_{max} at the fatigue limit can be 30 to 35% lower than Q_{max} at the static strength (extrapolated). This is a clear reminder that conservative adhesive bond designs should be based on fatigue behavior, not static strength.

Finally, some investigators have reported to us that fatigue crack initiation seems to be more sensitive to surface pre-treatment than crack propagation. Clearly, the methodology described herein shows some promise to test this hypothesis. Since the 90° bimaterial wedge seems to generate the smallest amount of scatter, it seems to be the optimal geometry to carry out this kind of investigation.

Acknowledgments

This work was funded by the National Science Foundation Science and Technology Center: High Performance Polymeric Adhesives and Composites, contract DMA 9120004. The authors express thanks to Brenda Jackson, Jia Qi and Huiying Zhang for help in specimen fabrication.

References

[1] Lefebvre, D. R. and Dillard, D. A., "A Stress Singularity Approach for the Prediction of Fatigue Crack Initiation in Adhesive Bonds. PART 1: Theory". Companion paper, this issue.
[2] Quick, S., *SAMPE NSTC* **28**, 1116 (1983).
[3] Fayard, J., Bignonnet, A. and Dang Van, K., Fatigue Design 1995, Vol. 1, VTT Symposium 155, Helsinki, Finland, September 1995, p. 239.
[4] Zhang, Z., Shang, J. K. and Lawrence, F. L., *J. Adhesion* **49**, 23 (1995).
[5] Shell Technical Report "*Epon Resin, Epoxy Bisphenol F 862*", Shell Chemical Company (1995).
[6] Timoshenko, S., *J. Opt. Soc. Am.* **11**, 233 (1925).
[7] Reedy, E. D. and Guess, T. R., *J. Adhesion Sci. Technol.* **10**, 33 (1996).
[8] Hattori, T., Sakata, S. and Murakami, G., *J. Electronic Packaging* **111**, 243 (1989).
[9] Tsai, M. Y. and Morton, J., *J. Strain Analysis* **29**(1), 137 (1994).
[10] Akisanya, A. R. and Fleck, N. A., *Int. J. of Fracture* **58**, 93 (1992).